

# UC Berkeley

## UC Berkeley Previously Published Works

### Title

Band-Gap Reduction in  $(\text{BiCrO}_3)_m/(\text{BiFeO}_3)_n$  Superlattices: Designing Low-Band-Gap Ferroelectrics

### Permalink

<https://escholarship.org/uc/item/4320z70t>

### Journal

Physical Review Applied, 10(4)

### ISSN

2331-7043

### Authors

Zhang, S  
Xiao, HY  
Peng, SM  
et al.

### Publication Date

2018-10-01

### DOI

10.1103/physrevapplied.10.044004

Peer reviewed

# **Band-Gap Reduction in $(\text{BiCrO}_3)_m/(\text{BiFeO}_3)_n$ Superlattices:**

## **Designing New Low-Band-Gap Ferroelectrics**

S. Zhang<sup>a</sup>, H.Y. Xiao,<sup>a,\*</sup> S. M. Peng<sup>b</sup>, G. X. Yang<sup>b</sup>, Z. J. Liu,<sup>c</sup> X.T. Zu<sup>a</sup>, S.

Li,<sup>d</sup> D. J. Singh,<sup>e</sup> L. W Martin,<sup>f,g</sup> and L. Qiao<sup>a,d\*</sup>

<sup>a</sup> *School of Physics, University of Electronic Science and Technology of China, Chengdu 610054, China*

<sup>b</sup> *Institute of Nuclear Physics and Chemistry, Chinese Academy of Engineering Physics, Mianyang 621900, China*

<sup>c</sup> *Department of Physics, Physics, Lanzhou City University, Lanzhou 730070, China*

<sup>d</sup> *School of Materials, University of New South Wales, Sydney, AU*

<sup>e</sup> *Department of Physics and Astronomy, University of Missouri, Columbia, Missouri 65211-7010, USA*

<sup>f</sup> *Department of Materials Science and Engineering, University of California, Berkeley, Berkeley, CA 94720 USA*

<sup>g</sup> *Materials Sciences Division, Lawrence Berkeley National Laboratory, Berkeley, CA 94720 USA*

Abstract□

Ferroelectric  $\text{BiFeO}_3$  is promising for photovoltaic applications, especially in regard to the exploitation of ferroelectric photovoltaic effects for charge separation. However, its large band gap limits efficient sunlight absorption. Here, we demonstrate a new strategy

to effectively tune the band gap of tetragonal BiFeO<sub>3</sub> via superlattice structuring with the ferroelectric BiCrO<sub>3</sub>. The (BiCrO<sub>3</sub>)<sub>m</sub>/(BiFeO<sub>3</sub>)<sub>n</sub> superlattices are found to exhibit conventional ferroelectric properties, but low fundamental band gaps; smaller than either of the parent materials. Using this approach, an optimized band gap of 1.6 eV is produced which matches closely the ideal band gap to achieve the Shockley-Queisser limit. First-principles calculations reveal that the unexpected band-gap reduction is induced by charge reconstruction due to lattice strain, octahedral distortion, and polarization discontinuity at the BiCrO<sub>3</sub> - BiFeO<sub>3</sub> interfaces. Ultimately, these results provide a new strategy, in the form of superlattice structuring, which could open the door to the creation of efficient ferroelectric photovoltaics.

Keywords: Band gap tuning; BiFeO<sub>3</sub>; Superlattice; Density functional theory;

\* Corresponding author. E-mail address:

[hyxiao@uestc.edu.cn](mailto:hyxiao@uestc.edu.cn) (H.Y. Xiao)

[liang.qiao@uestc.edu.cn](mailto:liang.qiao@uestc.edu.cn) (L. Qiao)

## I. INTRODUCTION

In the past several decades, researchers have been striving to open different corridors for the production of renewable energy. In this regard, photovoltaics (PVs) have been demonstrated to be a promising renewable energy technology to harvest solar energy [1-3], one of the most abundant energy sources available on Earth[4]. Generally, the performance of PV materials is quantified by the power conversion efficiency (PCE), which can be related to the photovoltage and photocurrent. Recently, building from initial interest in single-crystal and ceramic materials over four decades ago [5] □ a rejuvenation of interest in the so-called anomalous photovoltaic effect in non-centrosymmetric thin-film ferroelectrics has driven an urgent search for new materials in this space. Contrary to traditional semiconductor-based PVs, the photovoltage of ferroelectrics is not limited by their band gap, but can be a few orders of magnitude larger than the optical band gap of material itself [5,6]. In some cases, the photovoltage has been found to be  $> 10^4$  V [2,6]. Generally the photovoltage is proportional to the magnitude of the electric polarization [6-9]; however, the PCE of ferroelectric materials is normally limited by their small photocurrent density, typically on the order of  $\text{nA/cm}^2$ , which mainly originates from the large intrinsic band gap of these materials

(typically 3-4 eV) [2,10]. It is, therefore, of significant importance to lower the band gap of ferroelectric materials without affecting the ferroelectric polarization in an attempt to improve the PCE in PV applications. This is also of great importance for fully characterizing ferroelectric photovoltaic effects, including understanding the performance limits of these devices. While ferroelectric semiconductors do exist [11], for reasons yet to be understood, the largest effects have been observed in oxides, and therefore finding better oxide materials is a key challenge in the field.

A focus has been in  $\text{BiFeO}_3$  due to its intrinsic, relatively low band gap (2.67-3.1 eV) [12] and high polarization (90-158  $\mu\text{C}/\text{cm}^2$ ) [13-15]. Importantly,  $\text{BiFeO}_3$  has been widely investigated for PV applications and so far shows better PCE efficiency than most of other ferroelectric materials [2,16-20], making it a highly desirable ingredient in fabricating new ferroelectric photovoltaics. Despite these successes, however,  $\text{BiFeO}_3$  can only absorb UV light, which constitutes only ~20% of the entire solar spectrum; leaving most of the solar energy incident on Earth unexploited [21]. In epitaxial  $\text{BiFeO}_3$  thin films, there are several possible phases, including structures derived from monoclinic, triclinic, orthorhombic, and tetragonal parent structures. Of particular note is the tetragonal-like phase (which is actually a slightly monoclinically-distorted

tetragonal structure) which has a large  $c/a$  lattice parameter ratio of  $\sim 1.26$  and a giant spontaneous polarization approaching  $\sim 150 \mu\text{C}/\text{cm}^2$ . With this in mind, it is meaningful to reduce the band gap of tetragonal-like  $\text{BiFeO}_3$ , while **maintaining** the large spontaneous polarization, to enhance the PCE. On the other hand,  $\text{BiCrO}_3$  is another ferroelectric material, also with an active lone-pair on the bismuth cation [22], which is often used to tune the band gap and photocurrent of  $\text{BiFeO}_3$  [23-26], e.g. through alloying. We have recently studied alloyed  $\text{BiCrO}_3$ - $\text{BiFeO}_3$  films and found that chromium substitution can help to reduce the band gap by  $\sim 0.8 \text{ eV}$  for solid solution films and improves charge transport [27].  $\text{BiCrO}_3/\text{BiFeO}_3$  bilayer films, synthesized using a sol-gel technique, were found to exhibit a band gap of  $\sim 2.25 \text{ eV}$  (smaller than the value of  $2.64 \text{ eV}$  of  $\text{BiFeO}_3$ ) and a short circuit photocurrent density of  $0.08 \text{ mA}/\text{cm}^2$  (higher than the value of  $0.007 \text{ mA}/\text{cm}^2$  for a single-layer  $\text{BiFeO}_3$  film) [28]. Multiferroic  $\text{BiFeO}_3/\text{BiCrO}_3$  heterostructures have also been studied [10], and it was reported that the photocurrent density and photovoltage can be tuned by the thickness and the number of  $\text{BiFeO}_3/\text{BiCrO}_3$  bilayers and that the highest photocurrent density value ( $\sim 0.013 \text{ mA}/\text{cm}^2$ ) was recorded in 60-nm-thick heterostructures (including two  $\text{BiFeO}_3/\text{BiCrO}_3$  bilayers with each layer of thickness 15 nm).

More recently, significant band-gap reduction has been realized in double-perovskite  $\text{Bi}_2\text{CrFeO}_6$ , in which *B*-site-cation ordering controlled by film synthesis results in a remarkable PCE over 8.1% under AM 1.5G irradiation [21]; a new record for inorganic perovskites in conventional solar-cell applications. The mechanism of enhanced visible-light absorption and its correlation with cation ordering in the double-perovskite  $\text{Bi}_2\text{CrFeO}_6$ , however, is not clear. It is well known that for perovskites, achieving *B*-site-cation ordering is very difficult (and it is particularly sensitive to oxygen partial pressure and growth temperature) as the thermodynamic window allowing for the realization of such ordered states is extremely narrow. This has been shown true in a number of systems, including,  $\text{La}_2\text{VMnO}_6$  [29],  $\text{La}_2\text{CrFeO}_6$  [30], and  $\text{La}_2\text{NiMnO}_6$  [31], etc. On the other hand, superlattice ordering is also a powerful method to engineer ordered double-perovskite structures. For example, long-range ferromagnetism has been reported in  $\text{LaCrO}_3/\text{LaFeO}_3$  superlattices, which is unexpected, given that both  $\text{LaCrO}_3$  and  $\text{LaFeO}_3$  are antiferromagnetic [32]. Therefore, by creating an atomically-ordered state via superlattice structuring of the aforementioned  $\text{BiFeO}_3$  and  $\text{BiCrO}_3$ , one might expect to yield interesting electronic structure and material properties, distinct from alloys. There has been limited studies on  $\text{BiCrO}_3/\text{BiFeO}_3$  superlattices, and those which do exist

have focused mainly on traditional ferroelectric behavior. For example, using a scanning non-linear dielectric microscope, researchers found that the polarization in such superlattices is reversible and thus suggests that the superlattices are ferroelectric at room temperature [33]. The ground state properties of BiFeO<sub>3</sub>/BiCrO<sub>3</sub> superlattices, such as the electronic structure, intrinsic band gap, and ferroelectric polarization, are, however, not well developed.

Here, we report a density functional theory (DFT) investigation of the lattice geometrical and electronic properties of (BiCrO<sub>3</sub>)<sub>m</sub>/(BiFeO<sub>3</sub>)<sub>n</sub> superlattices, with a Hubbard-U correction for exchange correlation. Systematic study shows that the band gap of the superlattices is widely tunable, and can take values well below those of either component by itself, while still maintaining the ferroelectric polarization. Unexpectedly, the optimized band gap of ~1.6 eV for the BiCrO<sub>3</sub>/BiFeO<sub>3</sub> superlattice is not only smaller than both the single-layer BiFeO<sub>3</sub> and BiCrO<sub>3</sub>, but is also smaller than the equivalent Bi(Fe,Cr)O<sub>3</sub> alloy [27]. This surprising result is the consequence of charge reconstruction due to lattice strain, octahedral distortion, and polarization discontinuity at the superlattice interfaces. We also show that the ferroelectric and magnetic properties of the superlattice are not strongly affected.



These results demonstrate that superlattice structuring can be an effective strategy for the design of low band gap oxide semiconductors with fundamental band gaps much smaller than either parent materials, thus opening new perspectives for ferroelectric PVs.

## II. COMPUTATIONAL DETAILS

All of the spin-polarized calculations are carried out based on the DFT, using the Vienna ab-initio Simulation Package (VASP) code [34,35]. For the exchange and correlation energy, the Perdew-Burke-Ernzerhof functional [36] under the generalized gradient approximation (GGA) is employed. The on-site Coulomb interaction presented in  $3d$  states of transition-metal ions are corrected by the DFT+U (where U is the Hubbard energy) method [37], and we set  $U = 4$  eV for both Fe  $3d$  states and Cr  $3d$  states [27,38]. This is needed for realizing properties in accord with experiment for the bulk materials, with the exception that the band gap is still underestimated at this value of U. [Here, we consider the modified Becke-Johnson \(MBJ\) exchange potential to correct the underestimated band gap in electronic structure calculations \[39\].](#) A cutoff energy of 500 eV for plane-wave basis set and a  $4 \times 4 \times 4$  Monkhorst-Pack k-mesh for Brillouin-zone integrations are used for

structural relaxation. The convergence criteria for total energies and forces are  $10^{-4}$  eV and  $10^{-4}$  eV/Å, respectively. During the structural optimization, a full relaxation is employed. The spontaneous polarization is evaluated by simply summing the product of atomic displacements and corresponding Born effective charges (BECs) [40], which are calculated using density functional perturbation theory with a  $2 \times 2 \times 2$  Monkhorst-Pack k-mesh. For bulk BiFeO<sub>3</sub> (BFO) and BiCrO<sub>3</sub> (BCO), all computations are based on a  $2 \times 2 \times 2$  supercell containing 40 atoms. For the (BiCrO<sub>3</sub>)<sub>m</sub>/(BiFeO<sub>3</sub>)<sub>n</sub> ((BCO)<sub>m</sub>/(BFO)<sub>n</sub>) superlattices, which consist of m unit cells of BiCrO<sub>3</sub> alternating with n unit cells of BiFeO<sub>3</sub>, different alternating periodic cells, *i.e.*, (BCO)<sub>m</sub>/(BFO)<sub>1</sub> (m = 1, 2, 3, 4, 5) and (BCO)<sub>1</sub>/(BFO)<sub>n</sub> (n = 1, 2, 3, 4, 5), are considered.

### III. RESULTS AND DISCUSSION

#### A. Ground state properties of bulk BFO and BCO

The tetragonal-like phase of BFO with a space group of  $P4mm$  has a large  $c/a$  lattice parameter ratio (1.255-1.27) [12,41], where  $O_A$  and  $O_B$ , respectively, belong to the FeO and BiO layers [Fig.1 (a)]. Clearly, one Fe<sup>3+</sup> is coordinated by six O<sup>2-</sup> ions and an octahedra is formed. In the literature, it has been reported that the tetragonal-like BFO has G- and C-type antiferromagnetic spin states [38,42].

Schematic views of the spin configurations of BFO are illustrated [Fig. 1(b)-(c)]; in this work, both G- and C-type ordering are considered for bulk BFO and BCO.

For bulk BFO, the obtained lattice parameters of  $a = 3.755 \text{ \AA}$  and  $c/a = 1.300$  for G-type ordering are close to the calculated values of  $3.753 \text{ \AA}$  and  $1.303$ , respectively, for C-type ordering; both are in good agreement with the experimental values of  $3.72 \text{ \AA}$  and  $1.255$ [41], respectively. The calculated magnetic moment of Fe is  $4.136 \mu_B/\text{atom}$  for G-type ordering, agreeing well with the prior theoretical value of  $4.18 \mu_B/\text{atom}$  [43] and the experimental value of  $4.34 \mu_B/\text{atom}$  [44], and it is comparable to the result of  $4.130 \mu_B/\text{atom}$  for C-type ordering. Both G- and C-type ordered BFO exhibit direct band gaps and the values of band gap are  $1.62$  and  $1.71 \text{ eV}$ , respectively; which are smaller than the experimental data of  $3.1 \text{ eV}$  [12,45]. This is a generic problem in DFT, which persists in the PBE+U calculations, with  $U=4 \text{ eV}$ . Higher values of U **can correct the band gap**, but at the expense of ground state properties, and so we use  $U=4 \text{ eV}$ , and correct the band gap using **the MBJ approximation** [39,46] in further calculations for superlattices. For the DFT+U, which is widely used to address delocalization error, localize density on transition metals (TM) in low-spin and later TM and localize density away from TM in the other cases[47,48]. **Fig. ?? (a) shows**

the dependence of shift of TM partial charge  $\Delta q$  with  $U$  for bulk BFO and BCO. It is clearly that the localization of density is tendency away from TM in both G- and C-type BFO, indicating by the increased positive metal partial charges. Our calculations show that the geometrical structure, band structure and Fe magnetic moment of G- and C-type ordered tetragonal BFO are similar to each other, which is consistent with previous theoretical studies [38]. We also find that the total energy difference between G- and C-type ordered BFO is only 0.068 eV, indicating that the stability of these two orderings are comparable.

For bulk G- and C-type ordered BCO, the obtained magnetic moment of Cr and the lattice parameters are, like for the case of BFO, similar to each other [Table 1]. For G-type ordered BCO, the calculated lattice parameters are  $a = 3.926 \text{ \AA}$  and  $c = 4.073 \text{ \AA}$ , which are comparable to the experimental results of  $a = 3.888 \text{ \AA}$  and  $c = 3.902 \text{ \AA}$  [49]. On the other hand, the band gap of 0.94 eV for G-type ordered BCO is higher than the value of 0.69 eV for C-type ordered, and both values are smaller than the experimental value of 2.37 eV [28]. The calculated band gap of BCO (0.94 eV for G-type and 0.69 eV for C-type) is smaller than those of BFO (1.62 eV for G-type and 1.71 eV for C-type) consistent with the experimental results. [12,28]. In addition, the total energy of the G-type ordering

is 0.156 eV smaller than C-type ordering, *i.e.*, the G-type ordered BCO is energetically more preferable. Hence, in the subsequent calculations, we only consider the BFO and BCO with G-type ordering.

## **B. Geometrical structures of the superlattices**

Fig. 1(d) illustrates the geometrical structure for the optimized  $(\text{BCO})_1/(\text{BFO})_1$  superlattice. The optimized structural parameters of  $(\text{BCO})_m/(\text{BFO})_1$  and  $(\text{BCO})_1/(\text{BFO})_n$  superlattices are also presented [Table 2], including data for bulk BFO and BCO. The calculated lattice constant  $a$  and average  $c/a$  ratio as a function of  $m$  and  $n$  are also plotted [Fig. 2(a)]. It is found that the in-plane lattice constant  $a$  of  $(\text{BCO})_m/(\text{BFO})_1$  increases with increasing BCO layers, and the in-plane lattice constant of  $(\text{BCO})_1/(\text{BFO})_n$  decreases with increasing  $\text{BiFeO}_3$  layers, owing to the strain effect caused by the lattice mismatch between BFO and BCO. To the contrary, as can be seen [Fig. 2(b)], the average out-plane lattice constant  $c$  of the superlattices decreases with increasing BCO layers and increases with increasing BFO layers. For displacive ferroelectric materials, the  $c/a$  ratio reflects the tetragonal distortion, which is a consequence of the spontaneous polarization. Therefore, the observed increase of  $c/a$  ratio indicates an increase of relative displacement between

cations and anions, resulting in enhanced polarization [50,51]. The  $c/a$  ratio decreases with increasing BCO layers and increases with increasing BFO layers [Fig. 2(b)], indicating that the polarization of the  $(\text{BCO})_1/(\text{BFO})_n$  superlattices is larger than that of the  $(\text{BCO})_m/(\text{BFO})_1$  superlattices. This is seen directly in the polarization discussed in the next section. It is thus expected that the electrical and optical properties of the  $(\text{BCO})_m/(\text{BFO})_n$  superlattices can be adjusted by tuning the stacking period, which will alter the ground-state structure of superlattices due to strain effects [51].

The average interlayer distance  $\Delta d$  (the thickness of one monolayer, which is equivalent to the local out-of-plane lattice constant) and the bond angles  $\angle \text{O}_A\text{-Cr-O}_B$  and  $\angle \text{O}_A\text{-Fe-O}_B$  in BFO, BCO and the  $(\text{BCO})_m/(\text{BFO})_n$  superlattices are also summarized [Table 2]. We find that all the values of  $\Delta d_{\text{BFO}}$  for superlattices are smaller than the value of 4.879 Å for bulk BFO and the values of  $\Delta d_{\text{BCO}}$  are larger than the value of 4.073 Å for bulk BCO, indicating that the BFO in the  $(\text{BCO})_1/(\text{BFO})_n$  superlattices is compressed, while the BCO in the  $(\text{BCO})_m/(\text{BFO})_1$  superlattices is stretched along the [001] in comparison to their bulk values. This results from the interface stress caused by the large lattice mismatch (4.55%) between the BFO and BCO, since the lattice constant of BFO (3.755 Å) is much smaller than that of BCO (3.926 Å). For the  $(\text{BCO})_m/(\text{BFO})_1$

superlattices, as the number of BCO layers increases from 1 to 5,  $\Delta d_{\text{BFO}}$  decreases from 4.456 to 4.166 Å, and  $\Delta d_{\text{BCO}}$  decreases from 4.327 to 4.094 Å. Obviously, for the thicker BCO layers, the interlayer spacing of BFO is far from that in the bulk state and the interlayer distance between BCO layers becomes close to that in the bulk. Correspondingly, the  $\angle \text{O}_A\text{-Fe-O}_B$  angle deviates much more from the  $110.7^\circ$  in the bulk and the  $\angle \text{O}_A\text{-Cr-O}_B$  angle approaches the  $96.6^\circ$  in the bulk. These results suggest that the thicker BCO layers lead to significant compression of the BFO and large relaxation of BCO layers along the [001]. As for the  $(\text{BCO})_1/(\text{BFO})_n$  superlattices, when the BFO layer is increased in thickness from 1 to 5 unit cells, the BFO layer is compressed and the BCO layer is expanded considerably, resulting in  $\Delta d_{\text{BFO}}$  and  $\angle \text{O}_A\text{-Fe-O}_B$  approaching the bulk values for BFO and  $\Delta d_{\text{BCO}}$  and  $\angle \text{O}_A\text{-Cr-O}_B$  deviating significantly from the bulk values for BCO. Comparing the bond angles  $\angle \text{O}_A\text{-Cr-O}_B$  and  $\angle \text{O}_A\text{-Fe-O}_B$  in both the  $(\text{BCO})_1/(\text{BFO})_n$  and  $(\text{BCO})_m/(\text{BFO})_1$  superlattices, we find that both angles in the  $(\text{BCO})_1/(\text{BFO})_n$  superlattices are larger than those in the  $(\text{BCO})_m/(\text{BFO})_1$  superlattices, indicating that the distortion of the octahedra in the tetragonal lattice of the  $(\text{BCO})_1/(\text{BFO})_n$  superlattices is more significant, which results in a larger  $c/a$  ratio and polarization[50]. This is in good agreement with the discussions in above section. It is obvious that the induced

structural deformation and octahedral distortion in the  $(\text{BCO})_1/(\text{BFO})_n$  and  $(\text{BCO})_m/(\text{BFO})_1$  superlattices are different, indicating that they may exhibit different electronic structures and polarization.

### **C. Electronic structures of the superlattices**

Based on the optimized structures, we further calculate the band structures of the  $(\text{BCO})_m/(\text{BFO})_1$  and  $(\text{BCO})_1/(\text{BFO})_n$  superlattices. In this study, an approach of reverse scissor correction procedure is employed. This is an empirical correction consisting of a shift of the conduction regions up and can be applied to both GGA and LDA underestimated band gaps, especially in the determination of band-gap offsets for interfaces between different semiconductors [52-54]. Here we use a shift of 1.48 eV, which corrects the calculated band gap of BFO to the experimental value of 3.1 eV [12]. The variation of the band gap as a function of the number of BFO and BCO layers [Fig. 3] and the calculated band structures [Fig. 4] are plotted. The band gap of the superlattices is observed to decrease markedly with the number of layers of BFO and/or BCO in a given stack height [Fig. 3]. The band gap of the  $(\text{BCO})_1/(\text{BFO})_n$  superlattices are lower than that of the  $(\text{BCO})_m/(\text{BFO})_1$  superlattices for the same values of  $n$  and  $m$  ( $n, m > 1$ ). It may be caused by the lattice strain between BFO and BCO in superlattices, which results in



the BFO has tensile strain and the BCO has compressive strain in in-plane. Here, the Variation of band gap with the strain for bulk BFO and BCO are illustrated [Fig. ???]. The compressive strain indicated by negative values and the tensile strain indicated by positive values. The values of band gap increase with the increasing values of strain (%) for both BFO and BCO, indicating that the band gap of bulk BFO decreases under the tensile strain and that of BCO increases under compressive strain in in-plane. It is also shown that all the superlattices retain the direct character of BFO [Fig. 4]. The band-gap values for the superlattices are located within the range of 1.59-1.96 eV, which are unexpectedly smaller than the parent materials (e.g., 3.10 eV for direct-gap BFO and 2.42 eV for indirect-gap BCO). Furthermore, this value is also substantially smaller than that of the alloyed  $\text{Bi}(\text{Fe,Cr})\text{O}_3$  sample [27]. Similar results wherein the band gap of a composite compound is smaller than that of the parent materials have also been reported in superlattices of  $(\text{GaN})_1/(\text{ZnO})_1$  [55] and (0001)-oriented wurtzite  $(\text{GaN})_n/(\text{AlN})_n$  ( $n = 10, 12, 14$ ) [56] as well as nanocomposites of Carbon- $\text{ZrO}_2$  [57] and  $\text{NiO}:\text{TiO}_2$  system [58]. Furthermore, based on the results, it appears that the charge hybridization and carrier transport will mainly occur within the tetragonal plane rather than along the  $c$  axis, since the dispersion occurs along the G-X, X-M and M-G directions while the

bands are flat along the G-Z direction [59].

In order to understand the origin of the unexpected band-gap reduction, further electronic structure calculations are necessary. The partial charge density distributions at the valence-band maxima (VBM) and conduction-band minima (CBM) for BFO, BCO and the  $(\text{BCO})_1/(\text{BFO})_5$  and  $(\text{BCO})_5/(\text{BFO})_1$  superlattices are illustrated [Fig. 5]. It is found that holes at the VBM for  $\text{BiFeO}_3$  are mainly contributed by two types of oxygen anions, while the electrons at the CBM are mainly concentrated on the Bi and  $\text{O}_A$  and slightly on the Fe. For the BCO, the charge density distribution is remarkably different, the holes at the VBM are mainly gathered on the two types of O and Cr, while the electrons at the CBM are mainly contributed by the Bi and  $\text{O}_A$ . The different valence/conduction band characteristics of these two compounds originates from the different electron negativity of the transition-metal cations and thus the different electronic structures of BFO and BCO. The valence bands of BFO are mainly contributed by O 2p orbitals, whereas the O 2p and Cr 3d states dominate the valance bands of BCO [Fig. 6]. These results indicate that electron redistribution ~~may be resulted~~ should be expected when the BFO and BCO are ~~included in part of the same~~ superlattice structures. Comparing the charge distribution of the  $(\text{BCO})_1/(\text{BFO})_5$  superlattice with that of bulk BFO and BCO, we find that the holes at

the VBM for the  $(\text{BCO})_1/(\text{BFO})_5$  superlattices are mainly contributed by the interfacial Cr and O, and the electrons at the CBM are mainly gathered on the interfacial Fe, Bi, and a few  $\text{O}_A$  atoms. For the  $(\text{BFO})_5/(\text{BFO})_1$  superlattices, the charge distribution of the VBM and the CBM are similar to the  $(\text{BCO})_1/(\text{BFO})_5$  superlattices, where the holes at the VBM are mainly contributed by the Cr and  $\text{O}_B$  ions and the electrons at the CBM are mainly gathered on the Bi and  $\text{O}_A$  ions. The atomic projected density of state distribution [Fig. 6] also shows that there is a strong hybridization between the O  $2p$  and Cr  $3d$  states at the VBM of the  $(\text{BCO})_1/(\text{BFO})_5$  and  $(\text{BCO})_5/(\text{BFO})_1$  superlattices and the CBM of the  $(\text{BCO})_1/(\text{BFO})_5$  and  $(\text{BCO})_5/(\text{BFO})_1$  superlattices are mainly contributed by the Fe  $3d$ , O  $2p$ , and Bi  $6p$  orbitals. The Fermi level of the BFO is also shifted to higher energy when the superlattice structure is formed, accompanied by the upward shift of the valence bands [Fig. 6]. For the  $(\text{BCO})_1/(\text{BFO})_5$  superlattices, the conduction bands shift to lower energy as well. Consequently, the band gap of the  $(\text{BCO})_1/(\text{BFO})_5$  and  $(\text{BCO})_5/(\text{BFO})_1$  superlattices is much lower than that of BFO.

#### **D. Spontaneous polarization**

An excellent ferroelectric PV material should have not only a low band gap and high photocurrent, but also a large spontaneous

polarization. The polarization can be estimated by

$$\Delta P_{\alpha} \cong \sum_{j\beta} \frac{\partial P_{\alpha}}{\partial \mu_{j\beta}} (\mu_{j\beta} - \mu_{0j\beta}) = \frac{e}{\Omega} \sum_{j\beta} Z_{j\alpha\beta}^i \Delta \mu_{j\beta}, \quad \text{where } \Delta \mu_{j\beta} \text{ is the}$$

displacement of ions  $j$  in Cartesian direction  $\beta$ ,  $Z_{j\alpha\beta}^i$  is the Born effective charge tensor,  $e$  is the charge of an electron and the  $\Omega$  is the cell volume[40]. In this work, cubic BFO is used as the centrosymmetric reference structure, which is described by the zero subscript. In Fig. ??(b), the dependence of polarization with the values of  $U$  is shown. The value of  $U$  effects on the value of polarization. The polarization of superlattice is larger than that of BCO and smaller than that of BFO for all different values of  $U$ . Considered with ground state properties, we set the  $U=4.0$  eV for polarization calculations. The calculated polarization for the tetragonal-like BFO by this method is  $142.3 \mu\text{C}/\text{cm}^2$ ; agreeing well with the experimental data of  $150\text{-}158\mu\text{C}/\text{cm}^2$  [13,41] and other prior calculated values of  $136\text{-}145 \mu\text{C}/\text{cm}^2$  [60-62]. The polarization as a function of BFO and BCO layer number is plotted [Fig. 7]. It is shown that the polarization of all superlattices are located in the range of  $64.8\text{-}131.0 \mu\text{C}/\text{cm}^2$ . The polarization of the superlattices decreases with increasing the number of BCO layers, but increases

with increasing BFO layers, which is similar to the variation of the  $c/a$  ratio with layer number of both BFO and BCO. A similar dependence has been reported in tetragonal  $(\text{BaZrO}_3)_m/(\text{BaTiO}_3)_n$  superlattices which have a large  $c/a$  ratio and large polarization [51]. We find that the polarization of the superlattices are mainly contributed by the transition elements and the  $\text{O}^{2-}$  ions, and the contribution of  $\text{O}_A$  is larger than that of  $\text{O}_B$ . Besides, the direction of polarization of transition elements is in opposition to that of O and Bi atoms. In addition, the polarization of 92.9-131.0  $\mu\text{C}/\text{cm}^2$  for the  $(\text{BCO})_1/(\text{BFO})_n$  superlattices is larger than the polarization of 64.8-92.9  $\mu\text{C}/\text{cm}^2$  for the  $(\text{BCO})_m/(\text{BFO})_1$  superlattices, and the value of 131.0  $\mu\text{C}/\text{cm}^2$  for the  $(\text{BCO})_1/(\text{BFO})_5$  superlattices is the largest among all the investigated superlattices. This likely arises from the combined effects of lattice strain in the BFO layers due to lattice mismatch and the distorted octahedra in both the BFO and BCO.

The local polarization can also be described by the local displacement between transition-metal cations and oxygen anions in the superlattices[63]. The local displacement between the Cr/Fe and O ions for the  $(\text{BCO})_1/(\text{BFO})_5$  and  $(\text{BCO})_5/(\text{BFO})_1$  superlattices along the [001] direction is provided [Fig. 8]. It can be seen that both the displacements of the BFO and BCO part for the  $(\text{BCO})_1/(\text{BFO})_5$  and  $(\text{BCO})_5/(\text{BFO})_1$  superlattices fluctuate slightly with

increasing distance from the interface, and there is a sharp decrease at the interface, indicative of a sharp change in the polarization at the  $\text{BiFeO}_3/\text{BiCrO}_3$  interface. This polarization discontinuity has been observed in  $\text{BiFeO}_3/\text{SrTiO}_3$  [64],  $\text{LaAlO}_3/\text{PbTiO}_3$  [63], and  $\text{PbTiO}_3/\text{SrTiO}_3$  [65] heterostructures in which there is an internal electric field and a two-dimensional-like electronic gas is formed at the interface. In this study, the polarization discontinuity at the interface and the induced charge reconstruction also contribute to the remarkable reduction in the band gap for the  $(\text{BCO})_m/(\text{BFO})_n$  superlattices.

#### **IV. CONCLUSION**

In summary, this work provides a systematic DFT+U investigation of  $(\text{BCO})_m/(\text{BFO})_1$  and  $(\text{BCO})_1/(\text{BFO})_n$  superlattices ( $m, n=1, 2, 3, 4, 5$ ) to understand how the superlattice structuring and periodicity influences the geometrical structure and electronic properties. Due to the lattice mismatch between BCO and BFO, significant compression of the  $\text{BiFeO}_3$  layer and large relaxation of the BCO layers along the [001] are found for the  $(\text{BCO})_m/(\text{BFO})_1$  superlattices, and considerable expansion of the BCO layer and remarkable relaxation of the BFO layers are found for the  $(\text{BCO})_1/(\text{BFO})_n$  superlattices. Meanwhile, the octahedral distortion in the

(BCO)<sub>1</sub>/(BFO)<sub>n</sub> superlattices is found to be more significant than that in the (BCO)<sub>m</sub>/(BFO)<sub>1</sub> superlattices. For all the considered superlattices, the band gap decreases significantly with increasing number of layers of BFO and/or BCO, and the band gap of the (BCO)<sub>1</sub>/(BFO)<sub>n</sub> superlattices is lower than that of the (BCO)<sub>m</sub>/(BFO)<sub>1</sub> superlattices for any given value of n and m (n, m>1). Additionally, all the superlattices retain the direct character of the BFO. Surprisingly, the (BCO)<sub>m</sub>/(BFO)<sub>n</sub> superlattices show significant band-gap reduction by as much as 1.5 eV. The optimized band gap of 1.6 eV is not only smaller than both BFO and BCO, but also smaller than the alloyed BiFe<sub>x</sub>Cr<sub>y</sub>O<sub>3</sub> samples, thus implying good potential for visible-light absorption. The polarization is found to be 92.9-131.0 μC/cm<sup>2</sup> for the (BCO)<sub>1</sub>/(BFO)<sub>n</sub> superlattices and 64.8-92.9 μC/cm<sup>2</sup> for the (BCO)<sub>m</sub>/(BFO)<sub>1</sub> superlattices, among which the value of 131 μC/cm<sup>2</sup> for the (BCO)<sub>1</sub>/(BFO)<sub>5</sub> superlattice is the largest and comparable to the polarization of BFO. These results demonstrate that superlattice ordering can be a new strategy to design low-band-gap semiconductors with fundamental band gaps much smaller than either parent materials, thus opening new perspective for ferroelectric photovaltics.

## **ACKNOWLEDGEMENTS**

H.Y.X was supported by the NSAF Joint Foundation of China (Grant No. U1530129). Z.J. Liu was supported by National Natural Science Foundation of China (Grant No. 11464025) and the New Century Excellent Talents in University under Grant no. NCET-11-0906. L.Q. was supported by National Natural Science Foundation of China (Grant No. 1174044). D.J.S. was supported by the Department of Energy through the S3TEC Energy Frontier Research Center, award DE-SC0001299. L.W.M. acknowledges the support of the National Science Foundation under grant DMR-1608938. The theoretical calculations were performed using the supercomputer resources at TianHe-1 located at National Supercomputer Center in Tianjin.



## Reference

- [1] P. Lopez-Varo, L. Bertoluzzi, J. Bisquert, M. Alexe, M. Coll, J. Huang, J. Antonio Jimenez-Tejada, T. Kirchartz, R. Nechache, F. Rosei, and Y. Yuan, *Physical aspects of ferroelectric semiconductors for photovoltaic solar energy conversion*, Phys. Rep. **653**, 1 (2016).
- [2] S. Y. Yang, L. W. Martin, S. J. Byrnes, T. E. Conry, S. R. Basu, D. Paran, L. Reichertz, J. Ihlefeld, C. Adamo, A. Melville, Y.-H. Chu, C.-H. Yang, J. L. Musfeldt, D. G. Schlom, J. W. A. III, and R. Ramesh, *Photovoltaic effects in BiFeO<sub>3</sub>*, Appl. Phys. Lett. **95**, 062909 (2009).
- [3] B. Chen, J. Shi, X. Zheng, Y. Zhou, K. Zhu, and S. Priya, *Ferroelectric solar cells based on inorganic-organic hybrid perovskites*, J. Mater. Chem. A **3**, 7699 (2015).
- [4] Y. Liu, S. Wang, Z. Chen, and L. Xiao, *Applications of ferroelectrics in photovoltaic devices*, Sci. China Mater. **59**, 851 (2016).
- [5] C. Paillard, X. Bai, I. C. Infante, M. Guennou, G. Geneste, M. Alexe, J. Kreisel, and B. Dkhil, *Photovoltaics with Ferroelectrics: Current Status and Beyond*, Adv. Mater. **28**, 5153 (2016).
- [6] Y. Yuan, Z. Xiao, B. Yang, and J. Huang, *Arising applications of ferroelectric materials in photovoltaic devices*, J. Mater. Chem. A **2**, 6027 (2014).
- [7] S. Y. Yang, J. Seidel, S. J. Byrnes, P. Shafer, C.-H. Yang, M. D. Rossell, P. Yu, Y.-H. Chu, J. F. Scott, J. W. Ager, L. W. Martin, and R. Ramesh, *Above-bandgap voltages from ferroelectric*, Nat. Nanotechnol. **5**, 143 (2010).
- [8] V. M. Fridkin, *Bulk photovoltaic effect in noncentrosymmetric crystals*, Crystallogr. Rep. **46**, 654 (2001).
- [9] L. Pintilie, I. Vrejoiu, G. L. Rhun, and M. Alexe, *Short-circuit photocurrent in epitaxial lead zirconate-titanate thin films*, J. Appl. Phys. **101**, 064109, 064109 (2007).
- [10] J. Chakrabartty, R. Nechache, S. Li, M. Nicklaus, A. Ruediger, F. Rosei, and D. D. Viehland, *Photovoltaic Properties of Multiferroic BiFeO<sub>3</sub>/BiCrO<sub>3</sub>Heterostructures*, J. Am. Ceram. Soc. **97**, 1837 (2014).
- [11] Y. Li and D. J. Singh, *Properties of the ferroelectric visible light absorbing semiconductors: Sn<sub>2</sub>P<sub>2</sub>S<sub>6</sub> and Sn<sub>2</sub>P<sub>2</sub>Se<sub>6</sub>*, Phys. Rev. Mater. **1**, UNSP 075402, Unsp 075402 (2017).
- [12] P. Chen, N. J. Podraza, X. S. Xu, A. Melville, E. Vlahos, V. Gopalan, R. Ramesh, D. G. Schlom, and J. L. Musfeldt, *Optical properties of quasi-tetragonal BiFeO<sub>3</sub> thin films*, Appl. Phys. Lett. **96**, 131907 (2010).
- [13] K. Y. Yun, D. Ricinschi, T. Kanashima, M. Noda, and M. Okuyama, *Giant ferroelectric polarization beyond 150  $\mu\text{C}/\text{cm}^2$  in BiFeO<sub>3</sub> thin film*, Jpn. J. Appl. Phys. Part 2-Letters & Express Lett. **43**, L647 (2004).
- [14] C. Ederer and N. A. Spaldin, *Effect of epitaxial strain on the spontaneous polarization of thin film ferroelectrics*, Phys. Rev. Lett. **95**, 257601 (2005).
- [15] Y.-H. Chu, L. W. Martin, M. B. Holcomb, and R. Ramesh, *Controlling magnetism with multiferroics*, Mater. Today **10**, 16 (2007).
- [16] S. Gupta, M. Tomar, and V. Gupta, *Ferroelectric photovoltaic response to*

- structural transformations in doped BiFeO<sub>3</sub> derivative thin films*, Mater. Design **105**, 296 (2016).
- [17]Y. Sun, X. Liu, J. Zeng, J. Yan, D. Shi, and H. Liu, *Photovoltaic Effects in Polarized Polycrystalline BiFeO<sub>3</sub> Films*, J. Electron. Mater. **44**, 4207 (2015).
- [18]S. M. Young, F. Zheng, and A. M. Rappe, *First-principles calculation of the bulk photovoltaic effect in bismuth ferrite*, Phys. Rev. Lett. **109**, 236601 (2012).
- [19]P. P. Biswas, T. Chinthakuntla, D. Duraisamy, G. N. Venkatesan, S. Venkatachalam, and P. Murugavel, *Photovoltaic and photo-capacitance effects in ferroelectric BiFeO<sub>3</sub> thin film*, Appl. Phys. Lett. **110**, 192906, 192906 (2017).
- [20]M. M. Yang, Z. D. Luo, D. J. Kim, and M. Alexe, *Bulk photovoltaic effect in monodomain BiFeO<sub>3</sub> thin films*, Appl. Phys. Lett. **110**, 183902, 183902 (2017).
- [21]R. Nechache, C. Harnagea, S. Li, L. Cardenas, W. Huang, J. Chakrabartty, and F. Rosei, *Bandgap tuning of multiferroic oxide solar cells*, Nat. Photonics. **9**, 61 (2015).
- [22]R. Nechache, P. Gupta, C. Harnagea, and A. Pignolet, *Enhanced magnetism in epitaxial BiFeO<sub>3</sub>/BiCrO<sub>3</sub> multiferroic heterostructures*, Appl. Phys. Lett. **91**, 222908 (2007).
- [23]S. K. Singh, S. Shanthi, and H. Ishiwara, *Reduced leakage current in BiFeO<sub>3</sub>-BiCrO<sub>3</sub> nanocomposite films formed by chemical solution deposition*, J. Appl. Phys. **108**, 054102 054102 (2010).
- [24]S. Gepraegs, M. Opel, S. T. B. Goennenwein, and R. Gross, *Multiferroic materials based on artificial thin film heterostructures*, Phil. Mag. Lett. **87**, 141 (2007).
- [25]P. Couture, G. V. M. Williams, J. Kennedy, J. Leveneur, P. P. Murmu, S. V. Chong, and S. Rubanov, *Multiferroic nanocrystalline BiFeO<sub>3</sub> and BiCrO<sub>3</sub> thin films prepared by ion beam sputtering*, Int. J. Nanotechnol. **14**, 56 (2017).
- [26]J. W. Kim, C. M. Raghavan, J. W. Kim, and S. S. Kim, *Multiferroic properties of a BiCrO<sub>3</sub>/BiFeO<sub>3</sub> double-layered thin film prepared by chemical solution deposition*, Ceram. Int. **41**, 7211 (2015).
- [27]L. Qiao, S. Zhang, H. Y. Xiao, D. J. Singh, K. H. L. Zhang, Z. J. Liu, X. T. Zu, and S. Li, *Orbital controlled band gap engineering of tetragonal BiFeO<sub>3</sub> for optoelectronic applications*, J. Mater. Chem. C **6**, 1239 (2018).
- [28]C. Nie, S. Zhao, Y. Bai, and Q. Lu, *The ferroelectric photovoltaic effect of BiCrO<sub>3</sub>/BiFeO<sub>3</sub> bilayer composite films*, Ceram. Int. **42**, 14036 (2016).
- [29]S. Chakraverty, K. Yoshimatsu, Y. Kozuka, H. Kumigashira, M. Oshima, T. Makino, A. Ohtomo, and M. Kawasaki, *Magnetic and electronic properties of ordered double-perovskite La<sub>2</sub>V<sub>2</sub>MnO<sub>6</sub> thin films*, Phys. Rev. B **84**, 132411, 132411 (2011).
- [30]S. Chakraverty, A. Ohtomo, D. Okuyama, M. Saito, M. Okude, R. Kumai, T. Arima, Y. Tokura, S. Tsukimoto, Y. Ikuhara, and M. Kawasaki, *Ferrimagnetism and spontaneous ordering of transition metals in double perovskite La<sub>2</sub>CrFeO<sub>6</sub> films*, Phys. Rev. B **84**, 064436, 064436 (2011).
- [31]M. P. Singh, K. D. Truong, S. Jandl, and P. Fournier, *Long-range Ni/Mn structural*

- order in epitaxial double perovskite  $\text{La}_2\text{NiMnO}_6$  thin films, *Phys. Rev. B* **79**, 224421, 224421 (2009).
- [32] K. Ueda, H. Tabata, and T. Kawai, *Ferromagnetism in  $\text{LaFeO}_3$ - $\text{LaCrO}_3$  superlattices*, *Science* **280**, 1064 (1998).
- [33] N. Ichikawa, M. Arai, Y. Imai, K. Hagiwara, H. Sakama, M. Azuma, Y. Shimakawa, M. Takano, Y. Kotaka, M. Yonetani, H. Fujisawa, M. Shimizu, K. Ishikawa, and Y. Cho, *Multiferroism at Room Temperature in  $\text{BiFeO}_3/\text{BiCrO}_3(111)$  Artificial Superlattices*, *Appl. Phys. Express* **1**, 101302 (2008).
- [34] G. Kresse and J. Hafner, *Ab initio molecular-dynamics for liquid-metals*, *Phys. Rev. B* **47**, 558 (1993).
- [35] G. Kresse and J. Furthmüller, *Efficiency of ab-initio total energy calculations for metals and semiconductors using a plane-wave basis set* *Comp. Mater. Sci.* **6**, 15 (1996).
- [36] J. P. Perdew, K. Burke, and M. Ernzerhof, *Generalized Gradient Approximation Made Simple*, *Phys. Rev. Lett.* **77**, 3865 (1996).
- [37] V. I. Anisimov, F. Aryasetiawan, and A. I. Lichtenstein, *First-principles calculations of the electronic structure and spectra of strongly correlated systems: The LDA+U method*, *J. Phys.-Condens. Mat.* **9**, 767 (1997).
- [38] H. Dong, C. Chen, S. Wang, W. Duan, and J. Li, *Elastic properties of tetragonal  $\text{BiFeO}_3$  from first-principles calculations*, *Appl. Phys. Lett.* **102**, 182905, 182905 (2013).
- [39] F. Tran and P. Blaha, *Accurate Band Gaps of Semiconductors and Insulators with a Semilocal Exchange-Correlation Potential*, *Phys. Rev. Lett.* **102**, 226401, 226401 (2009).
- [40] J. B. Neaton, C. Ederer, U. V. Waghmare, N. A. Spaldin, and K. M. Rabe, *First-principles study of spontaneous polarization in multiferroic  $\text{BiFeO}_3$* , *Phys. Rev. B* **71**, 014113, 014113 (2005).
- [41] D. Ricinchi, K. Y. Yun, and M. Okuyama, *A mechanism for the  $150 \mu\text{C cm}^{-2}$  polarization of  $\text{BiFeO}_3$  films based on first-principles calculations and new structural data*, *J. Phys.-Condens. Mat.* **18**, L97 (2006).
- [42] O. Dieguez, O. E. Gonzalez-Vazquez, J. C. Wojdel, and J. Iniguez, *First-principles predictions of low-energy phases of multiferroic  $\text{BiFeO}_3$* , *Phys. Rev. B* **83**, 094105, 094105 (2011).
- [43] N. Feng, W. Mi, X. Wang, Y. Cheng, and U. Schwingenschlogl, *Superior Properties of Energetically Stable  $\text{La}_{2/3}\text{Sr}_{1/3}\text{MnO}_3$ /Tetragonal  $\text{BiFeO}_3$  Multiferroic Superlattices*, *ACS Appl. Mater. Inter.* **7**, 10612 (2015).
- [44] T. P. Comyn, T. Stevenson, M. Al-Jawad, S. L. Turner, R. I. Smith, A. J. Bell, and R. Cywinski, *High temperature neutron diffraction studies of  $0.9\text{BiFeO}_3(3)$ - $0.1\text{PbTiO}_3(3)$* , *J. Appl. Phys.* **105**, 094108, 094108 (2009).
- [45] H. L. Liu, M. K. Lin, Y. R. Cai, C. K. Tung, and Y. H. Chu, *Strain modulated optical properties in  $\text{BiFeO}_3$  thin films*, *Appl. Phys. Lett.* **103**, 181907 (2013).
- [46] D. Koller, F. Tran, and P. Blaha, *Merits and limits of the modified Becke-Johnson exchange potential*, *Phys. Rev. B* **83**, 195134, 195134 (2011).

- [47]Q. Zhao and H. J. Kulik, *Where Does the Density Localize in the Solid State? Divergent Behavior for Hybrids and DFT plus U*, Journal of Chemical Theory and Computation **14**, 670 (2018).
- [48]H. J. Kulik, *Perspective: Treating electron over-delocalization with the DFT plus U method*, Journal of Chemical Physics **142**, 240901 (2015).
- [49]D. H. Kim, H. N. Lee, M. Varela, and H. M. Christen, *Antiferroelectricity in multiferroic BiCrO<sub>3</sub> epitaxial films*, Appl. Phys. Lett. **89**, 162904, 162904 (2006).
- [50]T. Qi, I. Grinberg, and A. M. Rappe, *Correlations between tetragonality, polarization, and ionic displacement in PbTiO<sub>3</sub>-derived ferroelectric perovskite solid solutions*, Phys. Rev. B **82**, 134113, 134113 (2010).
- [51]M. P. K. Sahoo, Y. Zhang, and J. Wang, *Enhancement of ferroelectric polarization in layered BaZrO<sub>3</sub>/BaTiO<sub>3</sub> superlattices*, Phys. Lett. A **380**, 299 (2016).
- [52]S. Mamoun, A. E. Merad, and L. Guilbert, *Energy band gap and optical properties of lithium niobate from ab initio calculations*, Comp. Mater. Sci. **79**, 125 (2013).
- [53]M. Lannoo and M. Schluter, *Calculation of the Kohn-Sham potential and its discontinuity for a model-semiconductor*, Phys. Rev. B **32**, 3890 (1985).
- [54]L. Makinistian and E. A. Albanesi, *Ab initio calculations of the electronic and optical properties of germanium selenide*, J. Phys.-Condens. Mat. **19**, 186211, 186211 (2007).
- [55]M. R. Boufatah and A. E. Merad, *Structural stability, elastic and electronic properties of zincblende (GaN)(1)/(ZnO)(1) superlattice: Modified Becke-Johnson exchange potential*, Mat. Sci. Semicon. Proc. **19**, 179 (2014).
- [56]X. Y. Cui, B. Delley, and C. Stampfl, *Band gap engineering of wurtzite and zincblende GaN/AlN superlattices from first principles*, J. Appl. Phys. **108**, 103701, 103701 (2010).
- [57]E. Bailon-Garcia, A. Elmouwahidi, F. Carrasco-Marin, A. F. Perez-Cadenas, and F. J. Maldonado-Hodar, *Development of Carbon-ZrO<sub>2</sub> composites with high performance as visible-light photocatalysts*, Appl. Catal. B-Environ. **217**, 540 (2017).
- [58]S. A. Rawool, M. R. Pai, A. M. Banerjee, A. Arya, R. S. Ningthoujam, R. Tewari, R. Rao, B. Chalke, P. Ayyub, A. K. Tripathi, and S. R. Bharadwaj, *pn Heterojunctions in NiO:TiO<sub>2</sub> composites with type-II band alignment assisting sunlight driven photocatalytic H<sub>2</sub> generation*, Appl. Catal. B-Environ. **221**, 443 (2018).
- [59]H. J. Feng, K. Yang, W. Deng, M. M. Li, M. Z. Wang, B. Duan, F. Liu, J. S. Tian, and X. H. Guo, *The origin of enhanced optical absorption of the BiFeO<sub>3</sub>/ZnO heterojunction in the visible and terahertz regions*, Phys.Chem.Chem.Phys. **17**, 26930 (2015).
- [60]H. Matsuo, Y. Kitanaka, R. Inoue, Y. Noguchi, and M. Miyayama, *Heavy Mn-doping effect on spontaneous polarization in ferroelectric BiFeO<sub>3</sub> thin films*, Jpn. J. Appl. Phys. **54**, 10NA03 (2015).

- [61]J. X. Zhang, Q. He, M. Trassin, W. Luo, D. Yi, M. D. Rossell, P. Yu, L. You, C. H. Wang, C. Y. Kuo, J. T. Heron, Z. Hu, R. J. Zeches, H. J. Lin, A. Tanaka, C. T. Chen, L. H. Tjeng, Y. H. Chu, and R. Ramesh, *Microscopic Origin of the Giant Ferroelectric Polarization in Tetragonal-like BiFeO<sub>3</sub>*, Phys. Rev. Lett. **107**, 147602 (2011).
- [62]D. Ricinschi, K. Y. Yun, and M. Okuyama, *First-Principles Study of BiFeO<sub>3</sub> Films with Giant Polarization and Its Dependence on Structural Parameters*, Ferroelectrics **335**, 181 (2006).
- [63]P. X. Zhou, S. Dong, H. M. Liu, C. Y. Ma, Z. B. Yan, C. G. Zhong, and J. M. Liu, *Ferroelectricity driven magnetism at domain walls in LaAlO<sub>3</sub>/PbTiO<sub>3</sub> superlattices*, Sci. Rep. **5**, 13052, 13052 (2015).
- [64]Z. Zhang, P. Wu, L. Chen, and J. Wang, *First-principles prediction of a two dimensional electron gas at the BiFeO<sub>3</sub>/SrTiO<sub>3</sub> interface*, Appl. Phys. Lett. **99**, 062902, 062902 (2011).
- [65]L.-y. Wei, C. Lian, and S. Meng, *Prediction of two-dimensional electron gas mediated magnetoelectric coupling at ferroelectric PbTiO<sub>3</sub>/SrTiO<sub>3</sub> heterostructures*, Phys. Rev. B **95**, 184102, 184102 (2017).

Table 1. The structural parameters and band gap ( $E_g$ ) of BFO and BCO with G-type and C-type AFM spin states.  $\angle O_A-M-O_B$ : bond angle (M= Fe or Cr); MM: magnetic moment of Fe and Cr.

Compound		$a$ (Å)	$c$ (Å)	$c/a$	$\angle O_A-M-O_B$ (°)	$E_g$ (eV)	MM ( $\mu_B$ )
BFO	G-type AFM	3.75	4.87	1.30	110.7	1.6	4.136
		5	9	0			
	C-type AFM	3.75	4.89	1.30	110.9	1.7	4.130
		3	0	3			
	Exp. <sup>a,b,c</sup>	3.72	4.67	1.25		3.1	4.34
Other cal. <sup>d</sup>			5		1.9	4.18	
BCO	G-type AFM	3.92	4.07	1.03	96.6	0.9	2.944
		6	3	7			
	C-type AFM	3.92	4.08	1.04	96.7	0.6	2.923
		1	7	2			
	Exp. <sup>e,f</sup>	3.88	3.90	1.00		2.3	
	9	2	3		7		

<sup>a</sup>Ref. 40; <sup>b</sup>Ref. 44; <sup>c</sup>Ref. 43; <sup>d</sup>Ref. 42; <sup>e</sup>Ref. 28; <sup>f</sup>Ref. 47.

Table 2. The calculated structural parameters (the values of  $c$  and  $c/a$  is the average values of overall superlattices), average interlayer distance  $\Delta d$  and bond angles of BFO, BCO and  $(\text{BCO})_m/(\text{BFO})_n$  superlattices.

Compounds	$a(\text{\AA})$	$c(\text{\AA})$	$c/a$	$\Delta d_{\text{BF}}$	$\Delta d_{\text{BC}}$	$\angle \text{O}_A\text{-Cr-}$	$\angle \text{O}_A\text{-Fe-}$
				$o$ ( $\text{\AA}$ )	$o$ ( $\text{\AA}$ )	$\text{O}_B$ ( $^\circ$ )	$\text{O}_B$ ( $^\circ$ )
BFO	3.75	4.87	1.30	4.87	-		110.7
	5	9	0	9			
BCO	3.92	4.07	1.03		4.07	96.6	
	6	3	7		3		
$(\text{BCO})_1/$	3.85	4.39	1.13	4.45	4.32	100.7	105.0
$(\text{BFO})_1$	6	2	9	6	7		
$(\text{BCO})_2/$	3.90	4.17	1.06	4.24	4.14	97.91	101.1
$(\text{BFO})_1$	5	5	9	3	1		
$(\text{BCO})_3/$	3.91	4.13	1.05	4.20	4.11	97.4	100.2
$(\text{BFO})_1$	4	4	6	3	2		
$(\text{BCO})_4/$	3.91	4.11	1.05	4.18	4.10	97.2	99.8
$(\text{BFO})_1$	7	7	1	3	1		
$(\text{BCO})_5/$	3.92	4.10	1.04	4.16	4.09	97.0	99.5
$(\text{BFO})_1$	0	6	7	6	4		
$(\text{BCO})_1/$	3.80	4.66	1.22	4.70	4.57	104.8	108.3
$(\text{BFO})_2$	2	0	6	1	8		
$(\text{BCO})_1/$	3.78	4.74	1.25	4.76	4.68	106.1	109.2
$(\text{BFO})_3$	4	4	4	4	0		
$(\text{BCO})_1/$	3.77	4.77	1.26	4.79	4.74	106.6	109.5
$(\text{BFO})_4$	6	5	4	0	1		
$(\text{BCO})_1/$	3.77	4.79	1.27	4.80	4.75	107.1	109.8
$(\text{BFO})_5$	2	8	2	8	1		





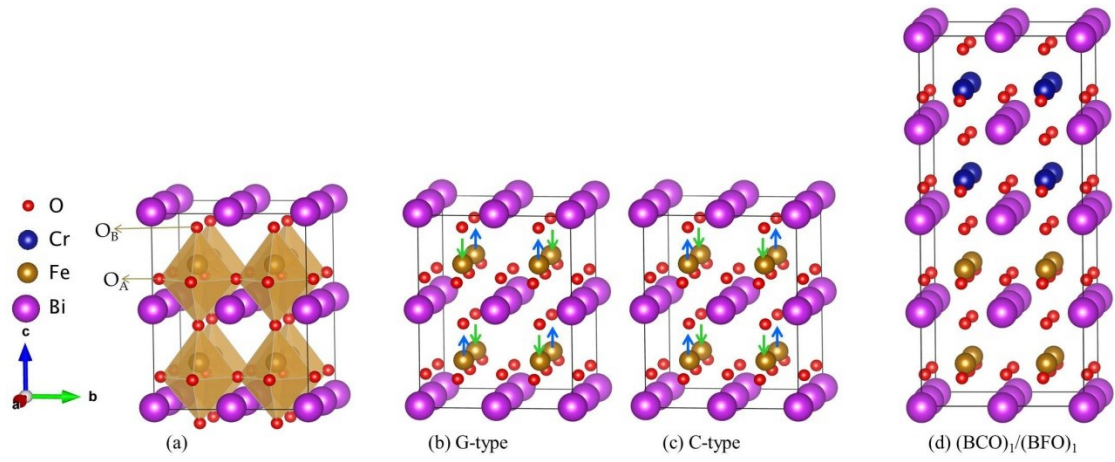


Figure 1. Schematic view of (a)  $2 \times 2 \times 2$  supercell for BFO; (b) BFO with a G-type AFM state; (c) BFO with a C-type AFM state and (d) optimized  $(\text{BCO})_1/(\text{BFO})_1$  superlattice.

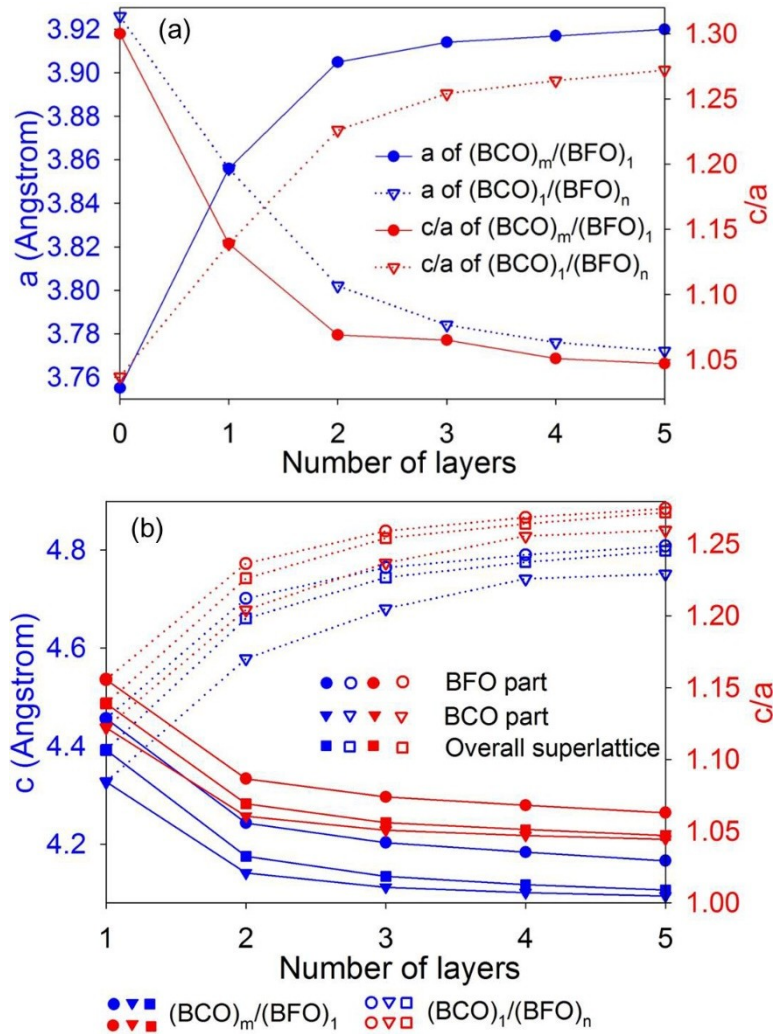


Figure 2. (a) Variation of lattice constants (blue) and  $c/a$  (red) for  $(\text{BiCrO}_3)_m/(\text{BiFeO}_3)_1$  and  $(\text{BiCrO}_3)_1/(\text{BiFeO}_3)_n$  ( $m, n = 0, 1, 2, 3, 4, 5$ ) as a function of number of layers. (b) Variation of out-plane lattice constants  $c$  (blue) and  $c/a$  (red) for  $(\text{BiCrO}_3)_m/(\text{BiFeO}_3)_1$  (solid) and  $(\text{BiCrO}_3)_1/(\text{BiFeO}_3)_n$  (hollow) ( $m, n = 0, 1, 2, 3, 4, 5$ ) as a function of number of layers. The circle sign is average of  $\text{BiFeO}_3$  part in superlattice, the triangle down sign is the average of  $\text{BiCrO}_3$  part in superlattice and the square sign is the average of overall

superlattices.

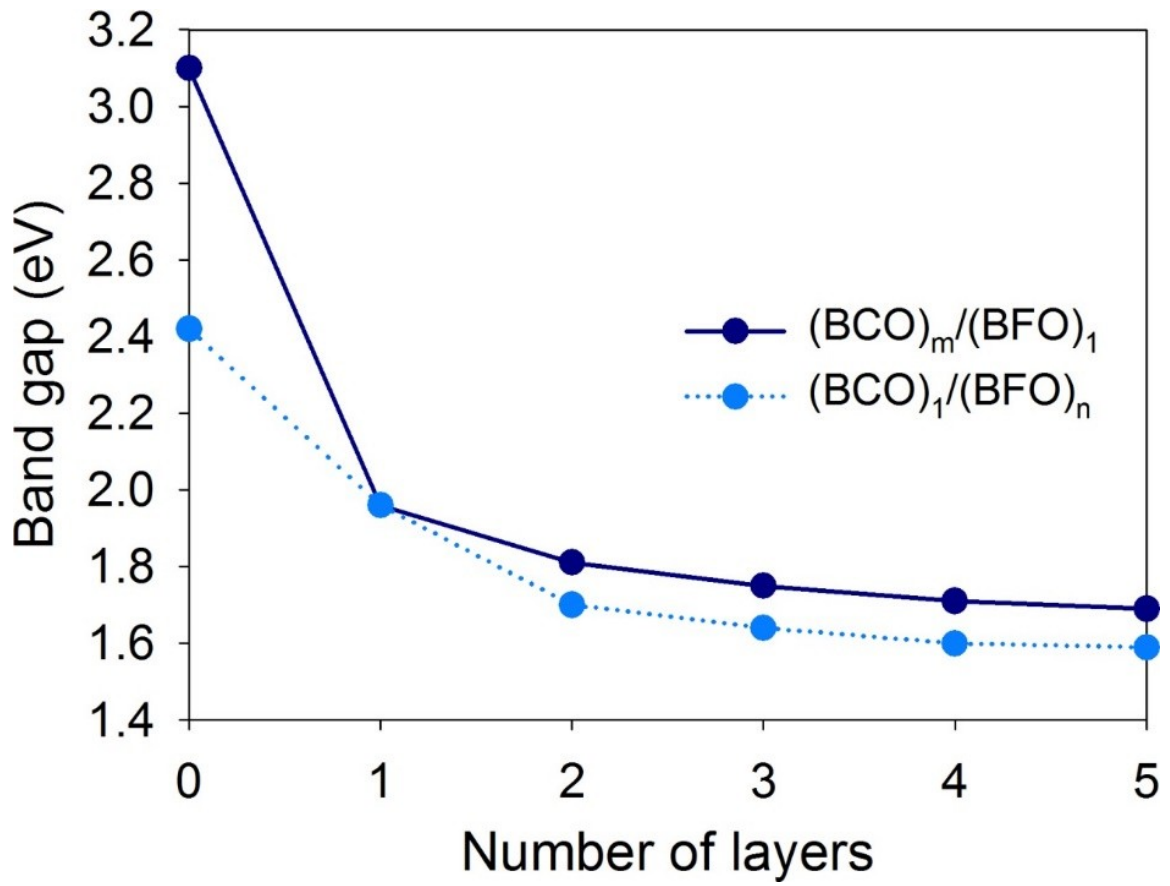


Figure 3. Variation of band gap for  $(\text{BCO})_m/(\text{BFO})_1$  and  $(\text{BCO})_1/(\text{BFO})_n$  ( $m, n = 1, 2, 3, 4, 5$ ) as a function of number of layers.

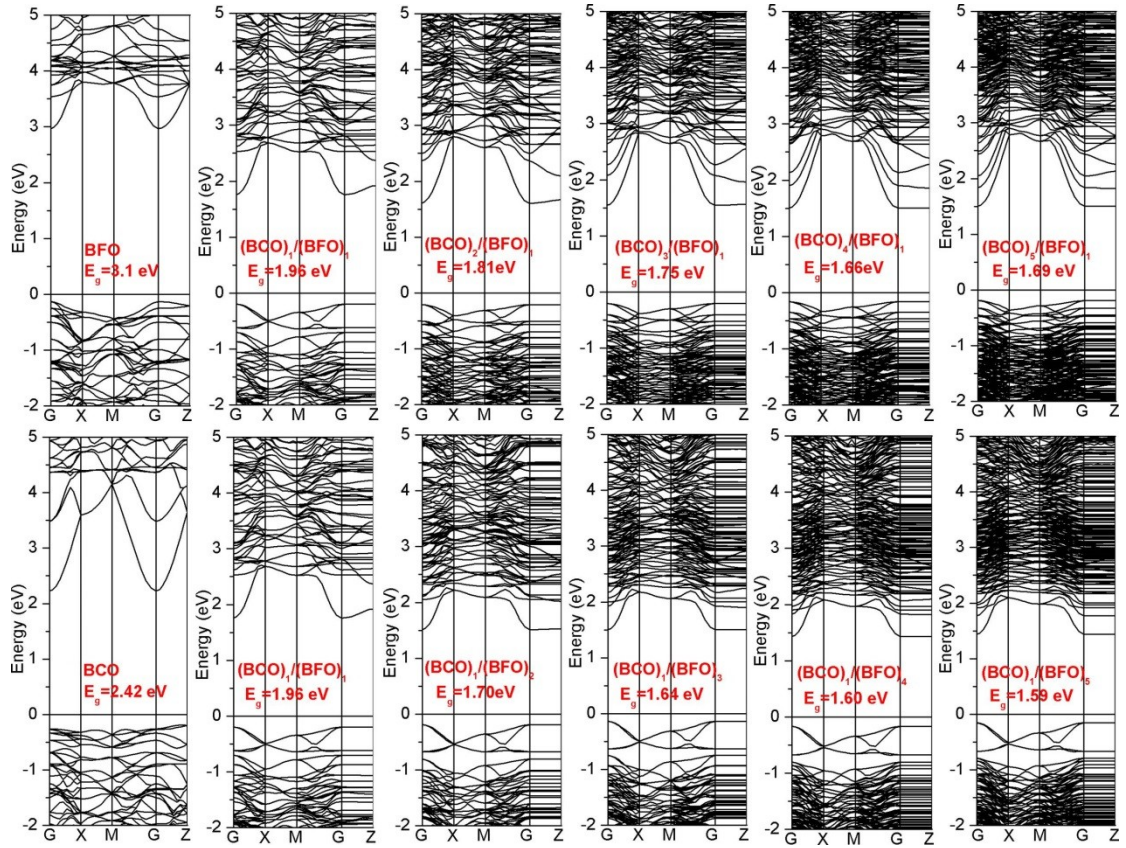


Figure 4. Band structure of bulk BFO, BCO,  $(\text{BCO})_m/(\text{BFO})_1$  and  $(\text{BiCrO}_3)_1/(\text{BiFeO}_3)_n$  ( $m, n = 1, 2, 3, 4, 5$ ) superlattices. The Fermi level is located at 0 eV.

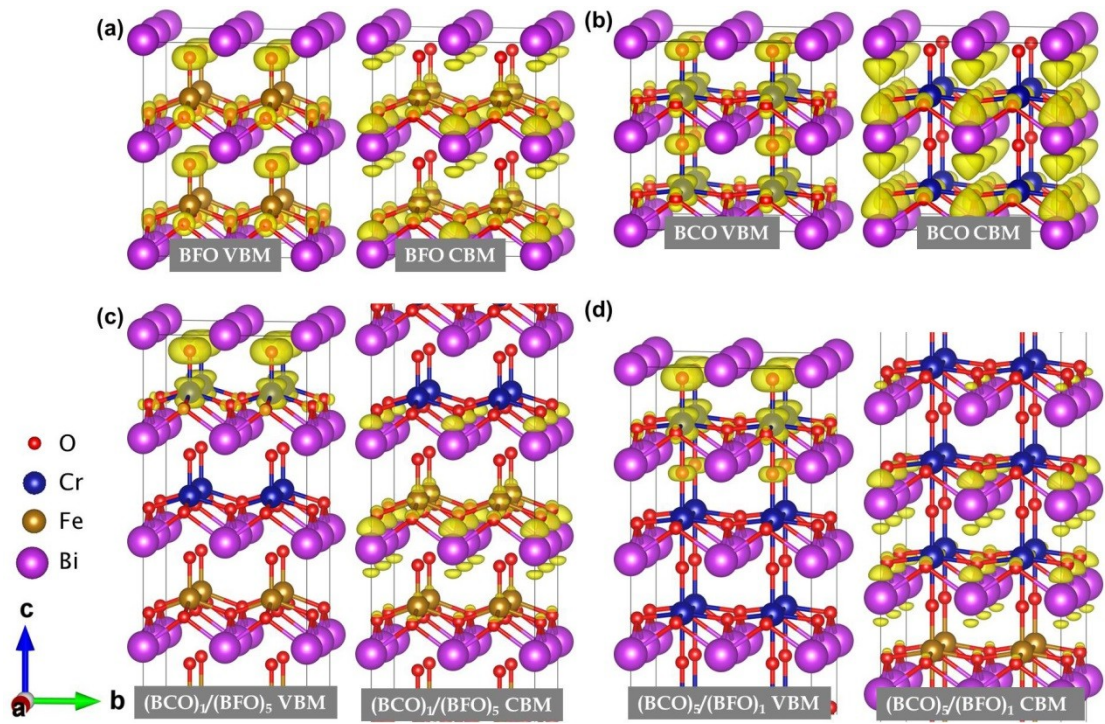


Figure 5. Partial charge density distributions at VBM (left) and CBM (right) for (a) BFO; (b) BCO; (c)  $(\text{BCO})_4/(\text{BFO})_5$  and (d)  $(\text{BCO})_5/(\text{BFO})_1$ .

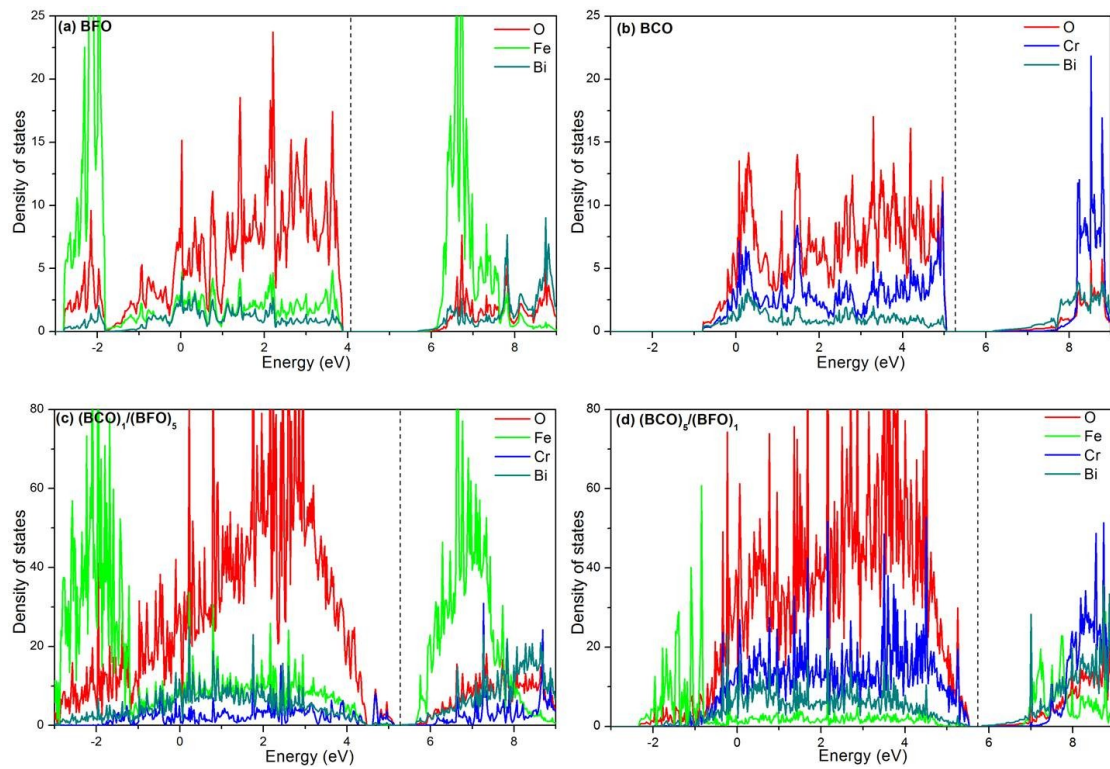


Figure 6. Atomic projected density of state distribution for (a)  $\text{BiFeO}_3$ ; (b)  $\text{BiCrO}_3$ ; (c)  $(\text{BiCrO}_3)_1/(\text{BiFeO}_3)_5$  and (d)  $(\text{BiCrO}_3)_5/(\text{BiFeO}_3)_1$ . The red line is the Fermi level. The Fermi level is located at the real level.

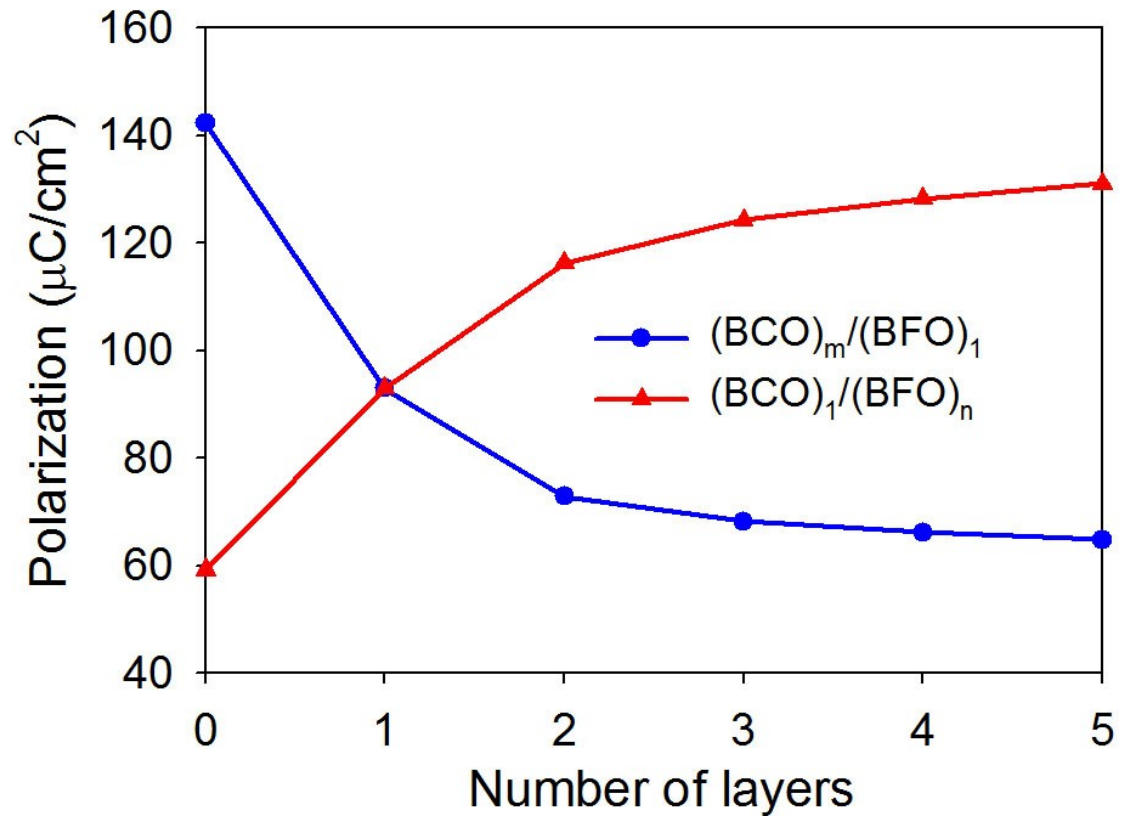


Figure 7. Variation of polarization for  $(\text{BCO})_m/(\text{BFO})_1$  and  $(\text{BCO})_1/(\text{BFO})_n$  ( $m, n = 0, 1, 2, 3, 4, 5$ ) as a function of number of layers.





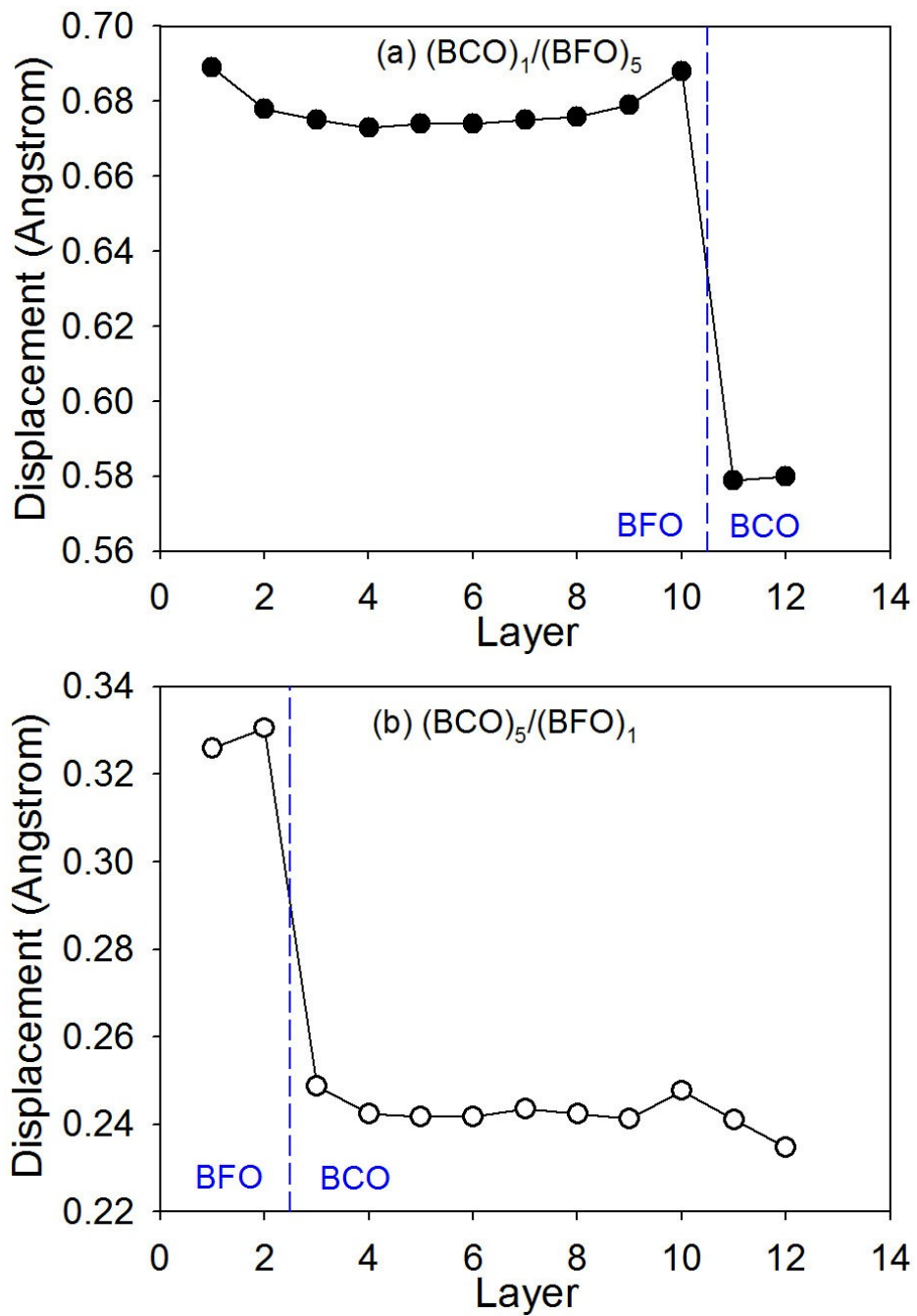


Figure 8. Local displacement between Fe/Cr ions and O ions for (a)  $(\text{BCO})_1/(\text{BFO})_5$  and (b)  $(\text{BCO})_5/(\text{BFO})_1$  superlattices.